Applied Catalysis B: Environmental 174–175 (2015) 67–76

Contents lists available at ScienceDirect

Applied Catalysis B: Environmental

journal homepage: www.elsevier.com/locate/apcatb

CuO/ZnO catalysts for methanol steam reforming: The role of the support polarity ratio and surface area

Cecilia Mateos-Pedrero [a,*], Hugo Silva [a], David A. Pacheco Tanaka [a,1], Simona Liguori [b], Adolfo Iulianelli [b], Angelo Basile [b], Adelio Mendes [a,**]

[a] LEPABE-Departamento de Engenharia Química, Faculdade de Engenharia da Universidade do Porto, Rua Dr. Roberto Frias, 4200-465 Porto, Portugal
[b] ITM-CNR, Via Pietro Bucci, Cubo 17C, c/o University of Calabria, 87030 Rende, CS, Italy

ARTICLE INFO

Article history:
Received 24 November 2014
Received in revised form 20 February 2015
Accepted 27 February 2015
Available online 28 February 2015

Keywords:
CuO/ZnO catalysts
Polarity ratio
Methanol steam reforming
CO selectivity
Pd-membrane

ABSTRACT

The effect of surface area and polarity ratio of ZnO support on the catalytic properties of CuO/ZnO catalyst for methanol steam reforming (MSR) are studied. The surface area of ZnO was varied changing the calcination temperature, and its polarity ratio was modified using different Zn precursors, zinc acetate and zinc nitrate. It was found that the copper dispersion and copper surface area increase with the surface area of the ZnO support, and the polarity ratio of ZnO strongly influences the reducibility of copper species. A higher polarity ratio promotes the reducibility, which is attributed to a strong interaction between copper and the *more polar* ZnO support. Interestingly, it was observed that the selectivity of CuO/ZnO catalysts (lower CO yield) increases with the polarity ratio of ZnO carriers. As another key result, CuO/ZnO_{Ac375} catalyst has proven to be more selective (up to 90%) than a reference $CuO/ZnO/Al_2O_3$ sample (G66-MR, Süd Chemie).

The activity of the best performing catalyst, $CuO/ZnO_{Ac\text{-}375}$, was assessed in a Pd-composite membrane reactor and in a conventional packed-bed reactor. A hydrogen recovery of *ca.* 75% and a hydrogen permeate purity of more than 90% was obtained. The Pd-based membrane reactor allowed to improve the methanol conversion, by partially suppressing the methanol steam reforming backward reaction, besides upgrading the reformate hydrogen purity for use in HT-PEMFC.

1. Introduction

The methanol steam reforming (MSR) reaction has received much attention in the past few decades as an attractive route of producing hydrogen for small-scale polymer electrolyte membrane fuel cells (PEMFC):

$$CH_3OH + H_2O \rightarrow 3H_2 + CO_2 \Delta H^\circ = 49.7\,kJ\,mol^{-1} \quad (1)$$

MSR catalysts are usually divided in two main groups: Cu-based and the more recent Pd-based ones [1]. Regardless, the catalyst type ZnO support has a ubiquitous presence. Although CuO/Zn-based catalysts are used in industry since the 1960s, the role of ZnO in these catalysts systems remains unclear despite the efforts made to elucidate its role [2–6]. For instance, Karim et al. investigated the effect of ZnO morphology on the reactivity of PdZnO catalysts for MSR [7], and concluded that the activity was higher for faceted ZnO materials [7]. In line with the former work, the theoretical studies by Smith et al. demonstrated that the polar crystalline surfaces of ZnO has null energetic barrier for both methanol and water dissociation [8]. On this basis, one could assume that ZnO with higher ratio of polar surfaces, namely higher polarity ratio, would lead to MSR catalysts with enhanced activity. This concept has in fact gained more attention as evident from the studies by Boucher et al. [9,10], who investigated the influence of the properties of various carriers (mainly shapes and defects) on the reactivity of Au-based catalysts for WGS and MSR reactions. These authors concluded that for different ZnO nanoshapes the activity increased when the binary catalysts were prepared with *more polar* supports (higher polarity ratio). Nevertheless, to our knowledge there is no study over CuO/ZnO catalysts that establishes a relation between the support polarity ratio and the selectivity toward MSR. However, this aspect is of crucial importance for fuel cell applications where the

Abbreviations: MR, membrane reactor; CR, conventional reactor; MSR, methanol steam reforming; WHSV, weight hourly space velocity; PEMFC, proton exchange membrane fuel cell.

* Corresponding author. Tel.: +351 22 508 1695.
** Corresponding author.
E-mail addresses: cmpedrero@fe.up.pt (C. Mateos-Pedrero), mendes@fe.up.pt (A. Mendes).
[1] Present address: Tecnalia, Parque Tecnológico de San Sebastián – Paseo Mikeletegi, 2. E-20009 Donostia, San Sebastián, Spain.

http://dx.doi.org/10.1016/j.apcatb.2015.02.039
0926-3373/

presence of CO should be minimized as much as possible since even ppm levels of CO irreversibly poison Pt electrodes.

Recently, a simple urea-assisted hydrothermal method for tailoring the physicochemical properties of ZnO materials was reported by the research team [11]. It was found that the specific surface area, morphology and polarity ratio of the resulting ZnO solids were strongly affected by the synthesis conditions employed [11], in particular, the presence and concentration of surfactant (Pluronic P123) and type of metal salt precursor (Zn-acetate *vs* Zn-nitrate). The main conclusions of this study were: (i) the addition of Pluronic P123 results in better dispersion of ZnO particles (hierarchical ZnO microflowers are formed), higher polarity ratio (higher ratio of (0 0 2) polar planes), and ZnO materials with enhanced surface area; (ii) the morphology, polarity ratio and reactivity are also affected by the Zn salt used as precursor. The use of Zn-nitrate led to urchin-like ZnO structures (ZnO microflowers were formed when using Zn-acetate) with lower polarity ratio (higher proportion of (1 0 0) non-polar planes) than their acetate derived counterparts. The ZnO sample with the highest polarity ratio (the acetate derived ZnO) also exhibited the highest photoactivity, which is *ca.* 2 times higher than that of the "*less polar*" (lower polarity ratio) nitrate derived ZnO. These results suggest that both samples have different reactivity, being higher for the ZnO with higher polarity ratio [11].

MSR reaction should be carried out at low temperature to exploit the favorable thermodynamics to yield low CO, but it is equilibrium limited and then, for high conversions, the back reaction penalizes the overall reaction rate. The use of a Pd-based membrane reactor allows hydrogen product to be continuously removed from the reaction medium and then enhances the overall reaction kinetics resulting in enhanced conversions and in the production of a high purity hydrogen stream. Low temperature PEMFCs require hydrogen with very low concentrations of CO; the automotive standard imposes a maximum CO concentration of 0.2 ppm (ISO 14687-2). This high purity hydrogen can be obtained using a Pd-based purification process or, with advantages, using a Pd-based membrane reactor. However, Pd-membranes are poisoned by CO, which adsorbs on the membrane surfaces inhibiting the hydrogen permeation [12]. Pd-based composite membranes are characterized by a thin Pd layer deposited onto porous substrates and show high permeability and selectivity to hydrogen [13–16]. A growing attention is then been devoted to Pd-composite membranes that have – among others – the advantage of lower cost and higher permeability because of the reduced palladium content utilized in these membranes [13–18]. Numerous studies deal with MSR reaction carried out in both dense and composite Pd-based MRs [17–25]. In most of them, it has been demonstrated that these MRs made possible higher performances than conventional packed bed reactors (CR) in terms of methanol conversion and hydrogen yield with the further benefit of producing high-grade hydrogen. Dense self-supported Pd–Ag membranes with a thickness of 50 μm and composite Pd-based membranes with Pd-layers thicker than 10 μm were used in previous studies of steam reforming of methanol [18,21–23]. This work uses a thin composite membrane of *ca.* 8 μm deposited onto a ceramic support and the direct contact of the catalyst with the composite membrane is assessed in terms of methanol conversion, hydrogen recovery and hydrogen permeate purity as well as permeation characteristics stability.

In this context, the first part of this work investigates the role of ZnO surface area and polarity ratio on the activity–selectivity of CuO/ZnO catalysts at low temperature. Two types of ZnO samples were prepared as detailed in [11] and used as supports of CuO/ZnO catalysts: a series of ZnO samples with different specific surface area and similar polarity ratio and a group of ZnO samples with similar specific surface area but different polarity ratio. It should be noted, however, that in the present work the term "polarity ratio" is used to refer the relative intensities of the polar and the nonpolar planes of ZnO, ($I_{(002)}/I_{(100)}$). A commercial isotropic würtzite ZnO from Sigma–Aldrich was taken as a reference and studied by XRD. The reference ZnO sample gave a value of 0.73 for the (0 0 2)/(1 0 0) intensity ratio, thus, intensity ratio values higher than the würtzite reference ($I_{(002)}/I_{(100)} = 0.73$) denote a higher polarity ratio, and consequently, a higher ratio of exposed polar facets, and *vice versa*.

The second part of this work evaluates the performances of the best CuO/$ZnO_{Ac\text{-}375}$ catalyst, among the ones reported in this work, in a Pd-membrane reactor.

2. Experimental

2.1. Preparation of ZnO supports

ZnO samples were prepared by a modified hydrothermal method as detailed elsewhere [11]. In a typical preparation, 1.1 g of zinc salt precursor (zinc acetate or zinc nitrate), 6 g of urea and 3 g of P123 Pluronic block copolymer were mixed in 100 mL of water. The pH was adjusted to 5 and the solution was stirred for 2 h under ambient conditions. Then, the mixture was poured into a teflon lined autoclave and kept at 90 °C for 24 h. The precipitate was thoroughly washed with distillated water and dried at 110 °C overnight. The resulting solid was calcined in a muffle furnace at given temperature for 30 min.

Table 1 shows the ZnO samples prepared. The following nomenclature for ZnO samples was used (Table 1) $ZnO_{x\text{-}CT}$, where: *x* denotes the zinc precursor, zinc-acetate (Ac) or zinc-nitrate (N) and CT represents the calcination temperature in °C (Table 1). Accordingly, the $ZnO_{Ac\text{-}375}$ sample was prepared from zinc-acetate as precursor and calcined at 375 °C for 30 min. SEM images of the series of ZnO materials ($ZnO_{Ac\text{-}CT}$) obtained at different calcination temperatures are shown in Fig. 1.

2.2. Preparation of CuO/ZnO catalysts

CuO/ZnO catalysts were prepared by impregnation of the ZnO supports with an aqueous solution of copper nitrate (the amount of copper calculated to achieve a nominal metal loading of 15 wt.%). The pH was adjusted to 6 by dropwise addition of ammonium

Table 1
Experimental parameters studied for the preparation of ZnO samples, calcination temperature series ($ZnO_{Ac\text{-}CT}$: Ac Zn-acetate as precursor; CT: calcination temperature); Zn-precursor series (ZnO_x-375: *x* stands for Zn-acetate (Ac) or Zn-nitrate (N); both samples were calcined at 375 °C).

Parameter studied	Range	Sample name	S_{BET} ($m^2\ g^{-1}$)	Polarity ratio* $I_{(002)}/I_{(100)}$
Calcination temperature (CT) (°C)	300	$ZnO_{Ac\text{-}300}$	64	0.76
	350	$ZnO_{Ac\text{-}350}$	71	0.78
	375	$ZnO_{Ac\text{-}375}$	80	1.10
	400	$ZnO_{Ac\text{-}400}$	54	0.80
Zn-precursor	Zn-acetate	$ZnO_{Ac\text{-}375}$	80	1.10
	Zn-nitrate	$ZnO_{N\text{-}375}$	77	0.60

*Ratio between XRD plane (0 0 2) and plane (1 0 0) – indicates the polarity degree of the ZnO carriers. The polarity ratio of an isotropic würtzite ZnO from Sigma–Aldrich was 0.73.

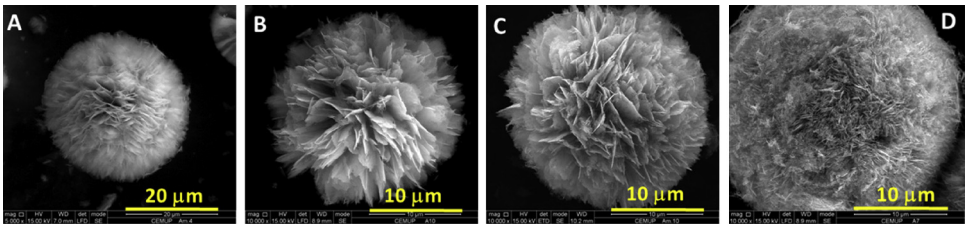

Fig. 1. Influence of the calcination temperature on the morphology of $ZnO_{Ac\text{-}CT}$ samples: (A) before calcination, and calcined in air at 300 (B), 375 °C (C) and 400 °C (D), respectively.

hydroxide. The resulting slurry was dried at 110 °C overnight and calcined at 360 °C during 8.5 h. As for ZnO carriers, CuO/ZnO catalysts will be denoted in terms of the ZnO supports calcination temperature (CT) and the type of zinc precursor used; thus, when zinc nitrate was used the catalyst was named $CuO/ZnO_{N\text{-}CT}$ and when prepared from zinc acetate it was named $CuO/ZnO_{Ac\text{-}CT}$, where CT denotes the calcination temperature in °C.

2.3. Materials characterizations

The specific surface area was measured by N_2 physisorption at −196 °C in a Quantachrome Autosorb-1 Instruments apparatus. The surface area (S_{BET}) was calculated using the Brunauer–Emmett–Teller (BET) equation. X-ray powder diffraction (XRD) analyses were carried using a Cu-Kα radiation (30 KV/15 mA and λ = 0.154 nm) in a Rigaku Miniflex 2 equipment. CuO crystallite size was assessed by the Debye–Scherrer equation, $D = K\lambda/\beta\cos\theta$, where D is the average size of the CuO crystallites, K is the Scherrer's constant 0.94, λ is the wavelength of X-ray, and β is the full width at half maximum. The XRD pattern was measured at ambient temperature and for the calcined samples of CuO/ZnO at a 2θ range of 10–80° with a step width of 0.06° s^{-1}. Temperature-programmed reduction (TPR) experiments were performed using a ChemBET Pulsar TPR/TPD equipped with a thermal conductivity detector (TCD). In a typical TPR experiment, approximately 50 mg of sample was held by quartz wool and placed in a U-shaped quartz reactor. The sample was heated from 50 °C to 400 °C at a heating rate of 5 °C min^{-1} under a flow of 5% H_2/Ar. Hydrogen consumption was measured by TCD. The copper dispersion was determined by temperature programmed desorption of H_2 (H_2-TPD), following a similar procedure as reported by Amorim de Carvalho et al. [26]. Accordingly, the sample was reduced under a flow of 5% H_2/Ar. Then, the sample was cooled to 0 °C with an ice bath and pure H_2 was passed during 1 h. Then, the temperature was lowered to −196 °C using liquid nitrogen under a pure H_2 flow (30 cm^3 min^{-1}). After 1 h, H_2 was switched to He flow (50 cm^3 min^{-1}) for 30 min. The temperature was then raised up to the 400 °C and desorption of H_2 was monitored by using a TCD detector. Copper dispersion is defined as the ratio of the surface copper atoms to the total copper atoms present in the catalyst.

2.4. MSR with a conventional rector

The activity and selectivity of the catalysts were determined for MSR reaction using an in house built set-up. Steam reforming of methanol was performed at atmospheric pressure in a tubular reactor (7.25 mm i.d.) placed inside an oven. The reaction temperature was recorded inside the packed bed reactor using a thermocouple. The reactor was loaded with 200 mg of catalyst (180–350 μm) diluted with 200 mg of glass spheres. Plug flow conditions were ensured keeping catalyst bed length to catalyst size ratio above 50 ($L_{reactor}/d_{particle} \geq 50$) and the reactor diameter to size ratio above 30 ($d_{reactor}/d_{particle} \geq 30$) [27]. Activity measurements were performed in the temperature range of 180–300 °C and space-time ratio of $W_{cat.}/F^0_{CH_3OH} = 83$ $kg_{cat.}mol^{-1}s$. Prior to the catalytic activity measurements, the catalyst was reduced *in situ* using a diluted hydrogen stream (40 vol.% of H_2 balanced with N_2), at 240 °C for 2 h. The gas feed flow rate was controlled by mass flow controllers from Bronkhorst (model F-201C, ±0.1 FS). Required flow rate of methanol aqueous solution was controlled using a controlled evaporation and mixing (CEM) system (Bronkhorst). The condensable reactants were separated from the gas mixture in a condenser at *ca.* 0 °C, placed outside the oven.

Hydrogen and carbon dioxide were analyzed in a quadruple mass spectrometer (Pfeiffer Vacuum OmniStar GSD 320). Trace amounts of carbon monoxide were measured using a CO infra-red analyzer (Signal Instruments, 7100 FM, accuracy: ±0.2 ppm). The methanol conversion (X_{CH_3OH}) and CO output molar fraction (Y_{CO}) were calculated by applying Eqs. (2) and (3).

$$\text{Methanol conversion}: X_{MeOH} = \frac{Q_{CO,out} + Q_{CO_2,out}}{Q_{CH_3OH,in}} \quad (2)$$

$$\text{COoutputmolarfraction}: Y_{CO} = \frac{Q_{CO,out}}{Q_{TOT,out}} \quad (3)$$

2.5. MSR with a composite Pd–Al_2O_3membrane reactor

A sketch of the Pd/Al_2O_3 membrane reactor (MR) used is shown in Fig. 2. The composite Pd-based membrane is made of a thin Pd layer (~7 μm) deposited *via* electroless plating onto a porous Al_2O_3 support. The membrane has been produced at Nanjing University of Technology (the porous Al_2O_3 support is from Gao Q Funct. Mat. Co.), and used at ITM–CNR, with 7.5 cm of total length and 5.0 cm of active length, 1.3 cm of O.D. It was housed in a stainless steel module, having 12 cm of length, 1.5 cm of O.D., equipped with two gaskets at both membrane ends for preventing permeate and retentate streams to mix. The MR annulus was packed with the CuO/ZnO catalyst. Prior to the reaction tests, the permeability of the composite Pd-membrane to hydrogen has been obtained at T = 300 °C and for a transmembrane pressure (ΔP) of 1.0 bar.

The performance of the MR has been first analyzed, in terms of methanol conversion and gas selectivity. The effect of temperature in the range 220–300 °C was assessed at 2.0 bar, ~0.95 h^{-1} weight hourly space velocity (WHSV) and H_2O/CH_3OH feed molar ratio equal to 2.5/1. The permeate pressure has been kept constant at 1.0 bar in the whole experimental campaign. Afterwards, the investigation has been focused on MR performance in terms of hydrogen recovery and hydrogen permeate purity by varying both reaction pressure and WHSV. The reaction pressure was varied from 1.5 bar to 2.5 bar, WHSV from 1.37 h^{-1} to 2.73 h^{-1}. The temperature was kept constant at 330 °C and H_2O/CH_3OH feed molar ratio equal to 1.5/1.

The MR has been heated up under helium and a P680HPLC pump (Dionex) has been used for supplying liquid methanol and water. The mixture was vaporized with nitrogen supplied at a constant flow rate of 22.0 mL/min and fed to the MR. The retentate stream was directed to a cold trap in order to condensate the unreacted

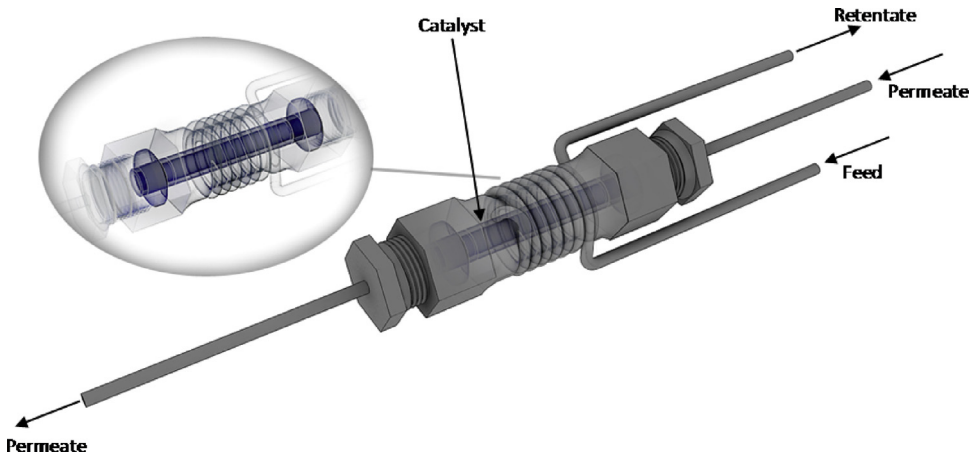

Fig. 2. Conceptual scheme of the composite Pd/Al_2O_3 MR with the catalyst (in powder form) packed into the MR annulus.

water and methanol. Both permeate and retentate stream compositions were analyzed using a temperature programmed HP 6890 GC with two thermal conductivity detectors, heated at 250 °C and using Ar as carrier gas. The GC was equipped with three packed columns: Porapack R 50/80 (8 ft 1/8 inch) and CarboxenTM 1000 (15 ft 1/8 inch) connected in series, and a Molecular Sieve 5 Å (6 ft 1/8 inch). The permeability of the membrane was obtained for monocomponent streams of H_2, N_2 and He using a bubble-flow meter; at least 10 experimental values were obtained.

Concerning the reaction tests, each experimental value obtained averages at least 10 measurements taken in a period of 120 min in steady-state conditions, with a relative difference smaller than 3%. Before reaction, the catalytic bed was reduced using a mixture of hydrogen and helium (1.1×10^{-2} mol min^{-1}) at 240 °C for 2 h.

The equations used for computing the parameters that characterize the Pd-based MR are indicated below.

Permeability characterizing parameters:

$$\text{Ideal selectivity}: \alpha_{H_2/i} = \frac{L_{H_2}}{L_i} \quad (4)$$

$$\text{Permeance}: L_i = \frac{J_i}{\Delta P_i} \quad (5)$$

where *i* can be He, N_2, H_2; J_i is the permeating flux of i-gas through the composite Pd/Al_2O_3 membrane.

Equations characterizing the reactor performance:

$$\text{Methanol conversion}: X_{MeOH} = \frac{Q_{CO,out} + Q_{CO_2,out}}{Q_{CH_3OH,in}} \quad (2)$$

$$\text{Output molar fraction}: Y_i = \frac{Q_{i,out}}{Q_{TOT,out}} \quad (3)$$

$$\text{Hydrogen re cov ery}: R_{H2_2} = \frac{Q_{H_2,permeate}}{Q_{H_2,retentate} + Q_{H_2,permeate}} \quad (6)$$

$$\text{Hydrogen permeate molar fraction}: y_{H_2} = \frac{Q_{H_2,permeate}}{Q_{TOT,permeate}} \quad (7)$$

where $Q_{CO,out}$, $Q_{CO_2,out}$ and $Q_{TOT,out}$ are the CO, CO_2 and total outlet molar flow rates, respectively, $Q_{H_2,retentate}$ and $Q_{H_2,permeate}$ are the H_2 outlet molar flow rates of retentate and permeate sides; and $Q_{TOT,retentate}$ and and $Q_{TOT,permeate}$ are the total outlet molar flow rates of retentate and permeate sides; $Q_{CH_3OH,in}$ is the inlet stream of methanol fed to the MR and $Q_{i,out}$ is the outlet molar flow rate of "i"-component (CO, CO_2, H_2).

3. Results and discussion

3.1. Physicochemical characterization

The XRD patterns of some representative ZnO supports and CuO/ZnO catalysts are shown in Fig. 3. All CuO/ZnO samples present well defined peaks which can be ascribed to ZnO (würtzite, JCPDS file no. 36-1451) and CuO (tenorite, JCPDS file no. 48-1548). It is important to note that the polarity ratio (defined as $I_{(002)}/I_{(100)}$) of ZnO supports remained unchanged after copper impregnation (Fig. 3): this evidences that copper deposition does not alter, at least in a significant way, the structure of the ZnO carriers, which maintain the initial preferential exposure of polar ($ZnO_{Ac\text{-}375}$) or nonpolar ($ZnO_{N\text{-}375}$) faces (Fig. 3).

As seen in Table 2, the average CuO crystallite was not significantly affected either by the Zn-precursor (Table 2, Fig. S1) or by the support calcination temperature. Most samples have similar crystallite size (16–18 nm, Table 2). The $CuO/ZnO_{Ac\text{-}400}$ sample has the largest CuO crystallite size (*ca.* 20 nm), which is likely due to the lower specific surface area of the ZnO support ($ZnO_{Ac\text{-}400}$, Table 1).

The temperature programmed desorption with H_2 was performed to evaluate the surface copper area the dispersion of copper. This technique was used as an alternative to the N_2O chemisorption since N_2O multilayer adsorption on copper oxide and N_2O dissociation by other catalyst components have been reported [26,28,29]. Additionally, the utilization of the H_2 TPD procedure appears to be easier and precise when compared to other methods.

Clearly both the copper surface area and the dispersion increase steadily with the surface area of ZnO support according to the following trend: $CuO/ZnO_{Ac\text{-}400} \ll CuO/ZnO_{Ac\text{-}300} < CuO/ZnO_{Ac\text{-}350} < CuO/ZnO_{N\text{-}375} \cong CuO/ZnO_{Ac\text{-}375}$ (Table 2, Fig. 5).

The H_2-TPR profiles of CuO/ZnO catalysts prepared with ZnO supports calcined at different temperatures are shown in Fig. S2A and B. The morphology of the TPR curves, intensity and reduction temperature for these groups of samples are different, indicating that the calcination temperature of the ZnO support affects the reducibility of copper species. According to the shape of the TPR curve, this series of samples can be grouped as follows: low temperature ($CuO/ZnO_{Ac\text{-}300}$ and $CuO/ZnO_{Ac\text{-}350}$, Fig. S2A) and high temperature samples ($CuO/ZnO_{Ac\text{-}375}$ and $CuO/ZnO_{Ac\text{-}400}$, Fig. S2B), henceforth labeled as LT- and HT-catalysts, respectively.

The LT-catalysts present very complex TPR profiles (Fig. S2A). A broad reduction peak is observed in the 200–300 °C temperature range, with maxima at 220 °C, 247 °C and 272 °C, and 214 °C, 233 °C and 257 °C (denoted as P_1, P_2 and P_3 in Table 2) for $CuO/ZnO_{Ac\text{-}300}$ and $CuO/ZnO_{Ac\text{-}350}$, respectively. A small H_2 uptake (HT-peak in Fig.

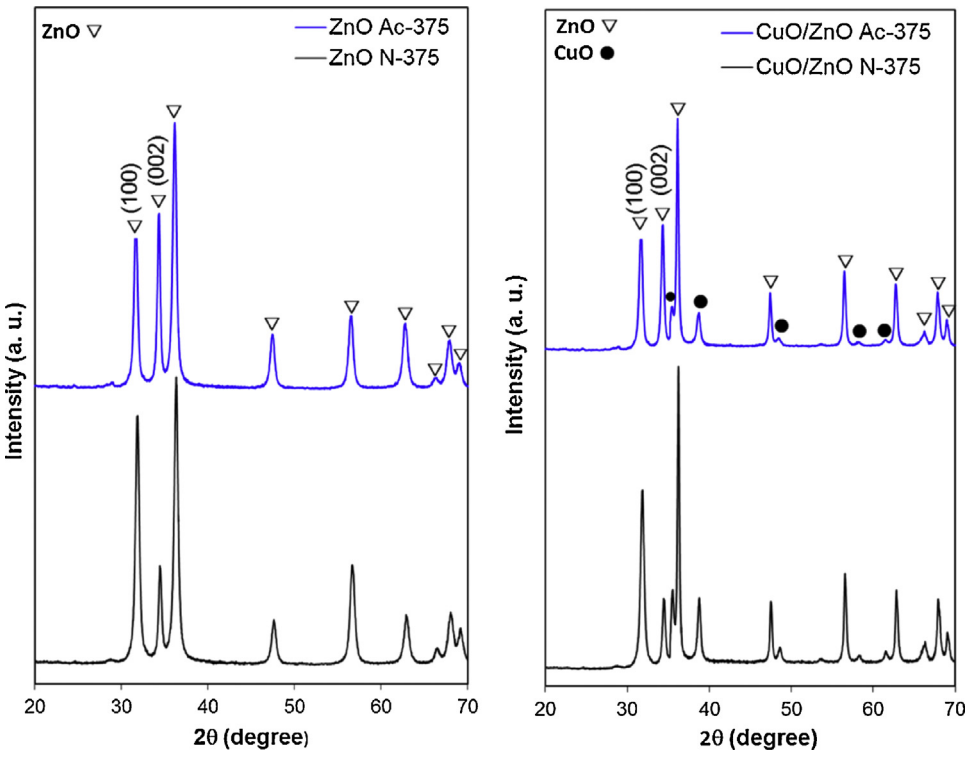

Fig. 3. XRD patterns for calcined CuO/ZnO catalysts.

S2A) between 300 and 350 °C is also seen. The existence of several peaks implies that different kinds of reducing copper oxide sites (with different environments, particle sizes, and/or oxidation state) coexist in the LT-catalysts. On the other hand, the broadness of the TPR curves shown in Fig. S2A could be likely due to the broad size distribution of the copper oxide particles.

The TPR profiles of the HT-catalysts (Fig. S2B) are dominated by a major peak centered at 173 °C and 202 °C for $CuO/ZnO_{Ac\text{-}375}$ and $CuO/ZnO_{Ac\text{-}400}$, respectively. As for the above-mentioned LT-catalysts, a small peak above 275 °C is observed (HT-peak in Fig. S2B). Despite their similarities, the $CuO/ZnO_{Ac\text{-}375}$ sample shows a great higher hydrogen consumption accompanied by a lower reduction temperature (Table 2), indicating an easier reducibility of Cu^{2+} cations on this sample. HT-catalysts exhibit reduction peaks considerably sharper and more symmetric than their LT-counterparts, suggesting smaller copper oxide particles with narrow size distribution.

According to the literature, the LT-peaks (150–300 °C) can be assigned to the reduction of copper oxide species in intimate contact with zinc oxide [30,31], since a strong interaction with ZnO can promote the reduction of CuO [30,31]. The small HT-peak (300–350 °C) may suggest the presence of a minor portion of CuO interacting less strongly with ZnO and/or larger CuO crystallites that need higher temperatures to be reduced.

In either case, all CuO/ZnO samples exhibit reduction temperatures much lower than that for bulk CuO. This fact is consistent with other published works reporting that the addition of promoters facilitates the reduction of copper oxide [30,31].

The TPR profiles for the catalysts prepared from different Zn-precursor ($CuO/ZnO_{N\text{-}375}$ and $CuO/ZnO_{Ac\text{-}375}$) displayed in Fig. 4A clearly highlight the large differences between both samples (curve shape and intensity, reduction temperature). The lower reduction temperatures along with the higher hydrogen consumption shown by $CuO/ZnO_{Ac\text{-}375}$ are clear indications of an enhanced reducibility of Cu^{2+} species. Such an improvement could be due to: (i) a higher dispersion (smaller size) of copper particles, and/or (ii) a strong interaction between copper species and the polar ZnO carrier. The first hypothesis seems unlike in view of the fact that both samples have comparable copper particle sizes (as shown by XRD and HRTEM, see Table 2 and Fig. S1) and dispersion (Table 2). On the other hand, both samples were prepared from ZnO carriers with very different polarity ratio, namely, preferential exposure of polar ($CuO/ZnO_{Ac\text{-}375}$) or nonpolar facets ($CuO/ZnO_{N\text{-}375}$). TPR results evidence that the reducibility of our CuO/ZnO catalysts is

Table 2
H_2-TPR data, CuO mean crystallite size and dispersion for CuO/ZnO samples.

Sample	d_{CuO}[a] (nm)	S_{Cu}[b] (m^2/g)	D[c] (%)	$T_{max.}$ (°C)				Overall TPR peak area (au)	Peak contribution to the overall TPR peak area (%)	
				P_1	P_2	P_3	P_4	A	LT-peak	HT-peak
$CuO/ZnO_{Ac\text{-}300}$	18	4.7	12	220	247	272	339	2276	79	21
$CuO/ZnO_{Ac\text{-}350}$	18	6.1	18	214	233	257	320	2878	88	12
$CuO/ZnO_{Ac\text{-}375}$	16	23.1	26	173	287	–	–	5470	91	9
$CuO/ZnO_{Ac\text{-}400}$	20	2.4	7	202	303	–	–	1762	81	19
$CuO/ZnO_{N\text{-}375}$	17	18.9	22	234	260	290	335	3017	87	13

[a] CuO mean crystallite size determined from Debye–Scherrer's method.
[b] Copper surface area determined by H_2-TPD experiments.
[c] Copper dispersion: ratio between amount of surface copper and total copper content.

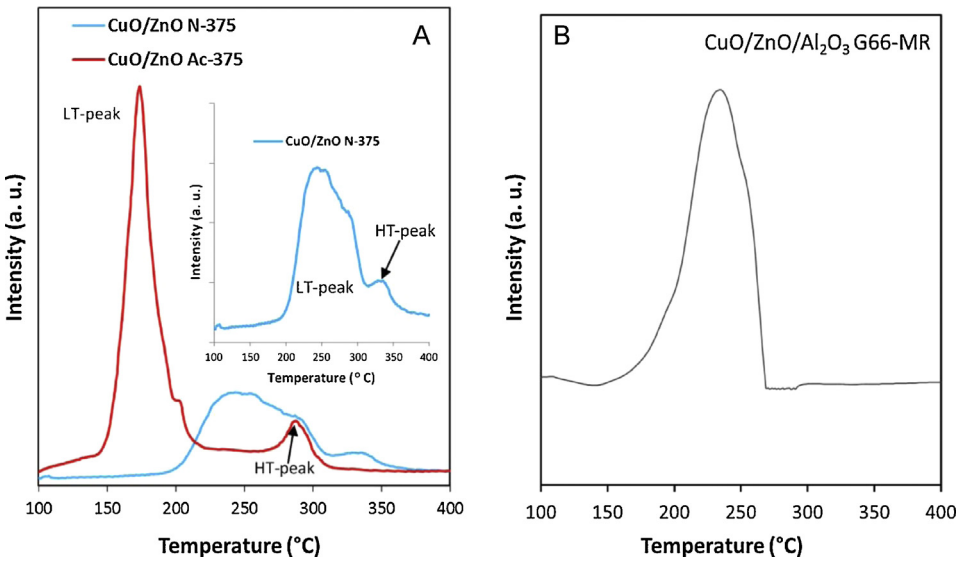

Fig. 4. TPR profiles of the CuO/ZnO samples prepared from different Zn-precursor, $CuO/ZnO_{Ac\text{-}375}$ and $CuO/ZnO_{N\text{-}375}$ (A) and commercial $CuO/ZnO/Al_2O_3$ (66/24/10 wt.%) catalyst (G66-MR) supplied by Süd Chemie (B).

notably influenced by the polarity ratio of ZnO carrier. Moreover, the symmetric shape of the LT-peak for the *more polar* sample, $CuO/ZnO_{Ac\text{-}375}$, suggests a narrow size distribution of copper species on this sample.

As indicated before, the LT-peak represents copper species intimately interacting with ZnO and from Fig. 4A is clear that the fraction of these species is higher in the *more polar* sample. Thus, it could be concluded that ZnO polar surfaces interacts strongly, at least to a higher extent than the *less polar* ZnO surfaces ($ZnO_{N\text{-}375}$), with highly dispersed copper particles modifying their electronic properties, and resulting in samples with enhanced reducibility. A recent study of Pd/ZnO catalysts pointed out in the same direction [32]. In fact, authors reported preferential formation of a PdZnβ alloy on polar ZnO facets [32], suggesting a different interaction between palladium particles and polar ZnO surfaces, as in the present case.

3.2. Catalytic activity of CuO/ZnO samples in the conventional reactor

The evolution of methanol conversion with the reaction temperature for some representative CuO/ZnO catalysts is presented in Fig. S3. Overall the methanol conversion, H_2 and CO_2 yields increase with temperature, as expected (Fig. S3, Table 3). Regardless, the catalyst and the temperature, H_2 and CO_2 are the main products, with CO formation initiating at 300 °C when methanol approaches complete conversion (Table 3). No CO was observed below 300 °C, excepting for $CuO/ZnO_{N\text{-}375}$ (Table 3). This is easily understood since CO is a by-product produced by endothermic reactions methanol decomposition (MD) and reverse water gas shift (RWGS) [1].

The catalytic activity at 180 °C as a function of the specific surface area of ZnO support and copper dispersion is illustrated in Fig. 5. Overall, the activity of the CuO/ZnO catalysts increases with the copper dispersion, with the latter increasing as the surface area of ZnO support does. ZnO supports with larger surface areas are able to better disperse Cu particles, leading to a higher number of exposed active sites (Cu sites) and consequently to a higher activity. It is also interesting to note that catalysts prepared from ZnO supports with similar surface areas ($CuO/ZnO_{Ac\text{-}375}$ and $CuO/ZnO_{N\text{-}375}$) have comparable copper dispersions and behave similarly in terms of activity (Fig. 5), in good agreement with our previous assumption.

Under the conditions of the present study, the dispersion of copper (or copper surface area) is the predominant factor governing the activity of CuO/ZnO catalysts in MSR. This agrees with other published results [33–35] reporting a linear correlation between the activity of Cu-based catalysts and the copper surface area.

On the contrary, there is no clear correlation between the CO production and the surface area of ZnO carriers or copper dispersion. In fact, all the catalysts obtained from ZnO with different SBET produce similar amounts of CO (Tables 1 and 3, series of CT catalysts). However, the two catalysts with similar surface areas but very different polarity ratio ($CuO/ZnO_{Ac\text{-}375}$ and $CuO/ZnO_{N\text{-}375}$) show the largest difference in selectivity. Clearly, the different selectivity of $CuO/ZnO_{Ac\text{-}375}$ and $CuO/ZnO_{N\text{-}375}$ samples cannot be ascribed to the ZnO surface area or copper dispersion.

The CO produced at 300 °C as a function of the ZnO polarity ratio is illustrated in Fig. 6. Data presented in this figure suggests that the selectivity (regarded as CO produced) is related to the polarity ratio of the ZnO supports, or in other words to the preferential exposure of polar or nonpolar facets of ZnO. In fact, copper catalysts supported on ZnOs with similar polarity ratios (Table 1), which in turn are very close to that of the würtzite reference (no anisotropy), produces nearly the same amount of CO (Table 3, Fig. 5). Conversely, copper catalysts supported on the ZnOs showing the highest dif-

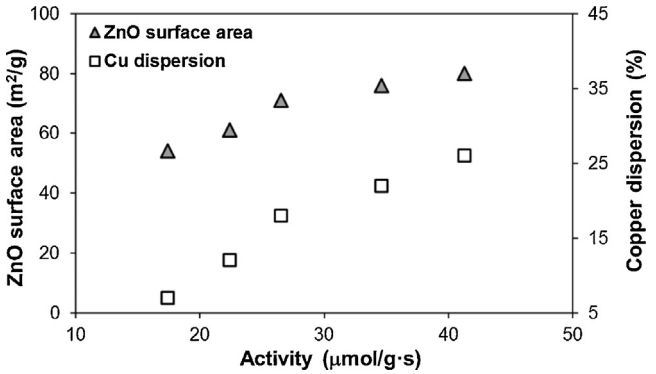

Fig. 5. Catalytic activity at 180 °C as a function of the specific surface area of ZnO carriers and copper dispersion.

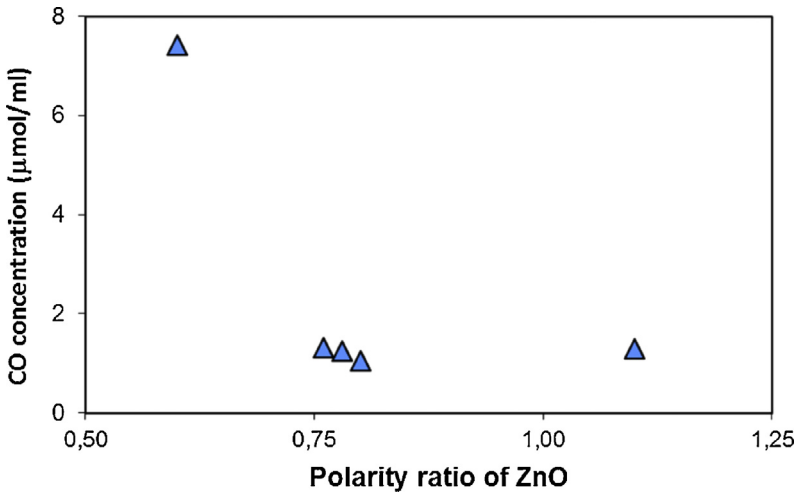

Fig. 6. Evolution of CO concentration (at 300 °C) as a function of the polarity ratio of ZnO carriers.

ference in polarity ratio, $ZnO_{N\text{-}375}$ and $ZnO_{Ac\text{-}375}$, (Table 1), which in turn are significantly different from that of the würtzite reference (anisotropy), show also the largest differences in selectivity (Table 3, Fig. 5): the lower the polarity ratio, the higher the CO production (Fig. 5). Thus, a *more polar* ZnO support gives more selective samples ($CuO/ZnO_{Ac\text{-}375}$), namely, producing lower CO amounts and *vice versa*.

The polarity ratio of ZnO is likely related to the presence of defects. Typical ZnO materials exhibit a würtzite structure with the polar planes corresponding to the basal planes of the hexagonal würtzite unit cell [36–38]. The würtzite configuration has preferential exposure of non-polar facets (lower polarity ratio). It is well-accepted that higher proportion of polar facets means also a higher number of defects, such as oxygen vacancies, that may play a crucial role in methanol and water activation [39,40]. It might be thought that the polar ZnO support itself is responsible for the enhanced MSR selectivity. In order to verify this hypothesis, MSR activity measurements were conducted over both polar ($ZnO_{Ac\text{-}375}$) and nonpolar ($ZnO_{N\text{-}375}$) ZnO samples under the same operating conditions as those used for CuO/ZnO samples. It was observed that both supports give very low methanol conversions (<3%) with almost complete selectivity toward CO_2 (so, negligible CO production – Table 3). Therefore, the ZnO support alone does not explain the enhanced selectivity.

It is then reasonable to assume that in the present case the nature of copper ZnO support interaction (evidenced by TPR) could account for the differences in selectivity.

ZnO was also found to affect the activity and selectivity of PdZnO catalysts in MSR reaction [32]. In line with this finding, a recent study about the influence of ZnO facets on the performances of Pd/ZnO catalysts for MSR also reached the same conclusion [41,42]. Authors reported that at comparable Pd/ZnO catalyst composition, the polar sample was more selective than the nonpolar one due to the preferential formation of the PdZnβ phase, which is selective toward CO_2, on the polar ZnO [41,42].

From the results compiled in Tables 1 and 3, it can be inferred that the polarity ratio of ZnO support does not exert any promoting effect on activity but clearly affects the selectivity (Fig. 5). TPR results evidenced strong interactions between copper and the *more polar* ZnO support ($ZnO_{Ac\text{-}375}$), which facilitates the reducibility of copper oxide leading to enhanced selectivity (decreases CO formation). This suggests that sites of particular reactivity may exist at the Cu–ZnO *polar* interface that are responsible for the higher selectivity of the *more polar* catalyst, $CuO/ZnO_{Ac\text{-}375}$. Despite our results do not allow identifying the exact role of the ZnO polarity ratio on the selectivity of CuO/ZnO catalysts, they clearly point out to its relevant role on the selectivity of the catalyst and suggest that the CuO–ZnO interface is involved in the MSR selectivity.

Another interesting finding of the present study is that the activity (per mass of metal) at 180 °C of the best in-house catalyst, $CuO/ZnO_{Ac\text{-}375}$, is up to 5-fold higher (Table 3) than that of a commercial $CuO/ZnO/Al_2O_3$ catalyst (66/24/10 wt.%; G66-MR, from Süd Chemie). Moreover, at comparable methanol conversion (300 °C, Table 3) the in-house sample produces considerably less CO (up to 90% lower, Table 3), further evidencing the high selectivity of $CuO/ZnO_{Ac\text{-}375}$ catalyst.

The first part of this study identified catalyst $CuO/ZnO_{Ac\text{-}375}$ to have the highest catalytic activity among the prepared catalysts and the highest selectivity of all catalysts. This catalyst was then

Table 3
Catalytic activity at 180 °C; methanol conversion, CO_2 and H_2 yields measured at 220 °C and 300 °C in the conventional fixed bed reactor; ($W_{cat.}/F^{\circ}_{CH_3OH} = 83\ kg_{cat.}\ mol^{-1}\ s$). CO reformate concentration at 300 °C is also shown in this table.

Sample	Activity (μmol/g_{met} s)	X_{CH_3OH} (%)		Y_{CO2} (%)		Y_{H_2} (%)		CO[b] (μmol/mL)
Temperature (°C)	180	220	300	220	300	220	300	300
$CuO/ZnO_{Ac\text{-}300}$	20.8	11.7	70.6	11.6	70.3	11.7	73.1	1.32
$CuO/ZnO_{Ac\text{-}350}$	22.6	13.8	74.8	13.7	73.6	13.8	76.5	1.29
$CuO/ZnO_{Ac\text{-}375}$	39.6	15.9 (<1)	82.2 (1.8)	15.7	80.9	16.1	84.1	1.06
$CuO/ZnO_{Ac\text{-}400}$	17.4	7.9	64.2	7.8	60.1	7.9	62.5	1.25
$CuO/ZnO_{N\text{-}375}$	24.1	14.7 (<1)	80.1 (2.4)	14.1	72.7	14.3	75.6	7.42
$CuO/Zn/Al_2O_3$[a]	7.65	63.8	90.1	60.3	82.1	62.1	83.5	9.61

[a] Commercial $CuO/ZnO/Al_2O_3$ (66/24/10 wt.%) catalyst (G66-MR) supplied by Süd Chemie. Values in brackets correspond to conversion and μmol of CO obtained when MSR tests were performed only with ZnO support.
[b] Corresponds to the CO reformate concentration at 300 °C, no CO was detected below this temperature(<0.05 μmol/mL) except for $CuO/ZnO_{N\text{-}375}$ sample that produces 1.67 μmol/mL and 3.01 μmol/mL of CO at 220 °C and 260 °C, respectively.

Table 4
Permeation characteristics of the fresh composite Pd/Al_2O_3 membrane at 300 °C and ΔP = 1.0 bar.

Pure gas (i)	J_i/mol m^{-2} s^{-1}	L_i/mol m^{-2} s^{-1} Pa^{-1}	α_{H_2}/i
H_2	1.42×10^{-1}	1.42×10^{-6}	1
N_2	2.36×10^{-5}	2.36×10^{-10}	>6000
He	4.29×10^{-5}	4.29×10^{-10}	~3300

selected to pack a Pd-based membrane reactor. The results obtained are presented and discussed in the next section.

3.3. Catalytic activity of $CuO/ZnO_{Ac\text{-}375}$ in the Pd/Al_2O_3 composite membrane reactor

Before the reaction tests, the permeation characteristics of the fresh Pd/Al_2O_3 membrane were investigated at T = 300 °C and ΔP = 1.0 bar. Table 4 shows the ideal selectivities obtained during the pure gas permeation tests.

The MSR on the composite Pd/Al_2O_3 MR were carried out by varying the temperature in the range 220–300 °C, at 2.0 bar, H_2O/CH_3OH feed molar ratio of 2.5/1 and WHSV = 0.95 h^{-1}. The objective of this first experimental campaign was evaluating the $CuO/ZnO_{Ac\text{-}375}$ catalyst performance in terms of activity and stability. Based on both permeate and retentate streams, Table 5 illustrates both methanol conversion and output molar fractions for different reaction temperatures. Though the composite Pd-based membrane has defects, besides hydrogen only CO_2 was found in the permeate stream. In particular, it is worth noting that a temperature increase allows two positive effects on the MR system: the first effect is related to the increase of the reaction rate with the temperature; the second one is due to the H_2 permeation through the membrane. In the latter case, at higher temperature the hydrogen permeation through the membrane is enhanced and, consequently, this induces a higher H_2 removal from the reaction to the permeate side, favoring the shift of the MSR reaction toward further products formation as well as higher methanol consume.

Fig. 7 highlights the stability of the catalyst as confirmed by the constant trend of H_2, CO, CO_2 selectivities with respect to time on stream up to 3 h of operation at steady state conditions. A similar trend was confirmed in all the MR experimental tests of this work, suggesting that the catalyst is stable under long time operation.

3.3.1. Pressure effect

The second campaign of experiments aimed to obtain high grade and high yields of hydrogen in permeate side. The reaction tests were carried out at 330 °C, feed molar ratio equal to 1.5/1, WHSV = 2.73 h^{-1} and by varying the reaction pressure between 1.5 and 2.5 bar. Table 6 shows the permeated hydrogen purity and the hydrogen recovery at 330 °C and at various reaction pressures.

The hydrogen recovery increases with the reaction pressure, overcoming 65% at 2.5 bar. Indeed, the highest reaction pressure maximizes the permeation driving force to hydrogen favoring the hydrogen permeation and then the hydrogen recovery. Nevertheless, the permeated hydrogen purity decreases with the reaction pressure. The composite palladium membrane should have pinholes that allow the diffusion/convection of other gas species. As the reaction pressure increases, more hydrogen is removed from the reaction medium making its permeation driving force to decrease. At the same time, the driving force to the other gas species increases, causing the purity of hydrogen at the permeate side to decrease. On the other hand, no CO was detected in the permeate side, as shown in Table 7.

Table 5
Methanol conversion (into gas) and output molar fractions (H_2, CO and CO_2) at different temperatures, WHSV = 0.95 h^{-1} and transmembrane pressure = 1.0 bar

Overall product molar fraction (%)	T = 220 °C	T = 260 °C	T = 300 °C
H_2	74.56	74.46	74.18
CO	0.75	0.88	1.25
CO_2	24.69	24.66	24.57
CH_3OH conversion (%)	12.4	47.1	97.4

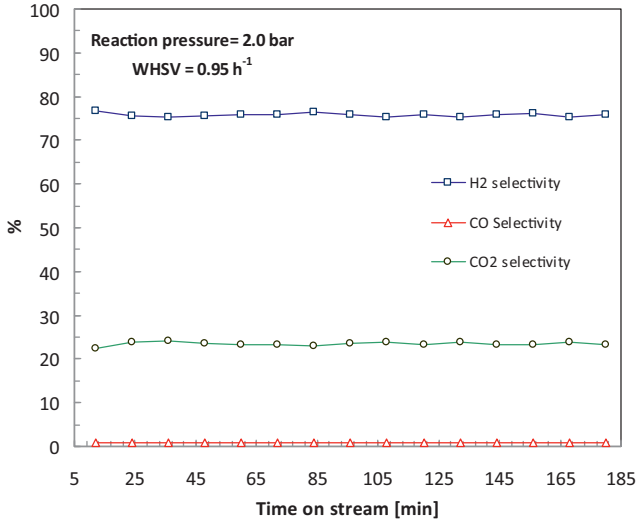

Fig. 7. Overall product molar fraction *vs* time on stream for MSR reaction in the Pd/Al_2O_3 MR at T = 220 °C, transmembrane pressure = 2.0 bar, WHSV = 0.95 h^{-1}, H_2O/CH_3OH = 2.5/1.

Table 6
Hydrogen permeate purity and hydrogen recovery *vs* reaction pressure at 330 °C, H_2O/CH_3OH = 1.5/1 and WHSV = 2.73 h^{-1} during MSR reaction in the Pd/Al_2O_3 MR.

Pressure (bar)	H_2 permeate purity (%)	H_2 recovery (%)
1.5	90	57
2.0	90	62
2.5	88	64

Table 7
Flow rates of the gases present in the permeate stream at different reaction pressure during MSR reaction at 330 °C, WHSV = 2.73 h^{-1}.

	Reaction pressure (bar)		
Flow rate gas in the permeate (mL min^{-1})	1.5	2.0	2.5
H_2	1.27	1.90	1.97
CO_2	0.11	0.16	0.2

3.3.2. WHSV effect

Hydrogen recovery and hydrogen permeate purity have been determined as a function of the WHSV at T = 330 °C, 2.5 bar reaction pressure and H_2O/CH_3OH feed molar ratio equal to 1.5/1. Table 8 shows that, as expected, the hydrogen recovery increases when WHSV decreases (higher residence times); the hydrogen recovery increased to around 75% at 1.37 h^{-1}.

Table 8
Hydrogen permeate purity and hydrogen recovery *vs* WHSV at 330 °C, H_2O/CH_3OH = 1.5/1 and reaction pressure = 2.5 bar during MSR in a Pd/Al_2O_3 MR.

WHSV (h^{-1})	H_2 permeate purity (%)	H_2 recovery (%)
1.37	88	72
2.05	88	66
2.73	87	63

Table 9
Permeation characteristics of the composite Pd/Al_2O_3 membrane at the end of the whole experimental campaign at 300 °C and ΔP = 1.0 bar.

Pure gas (i)	J_i/mol m^{-2} s^{-1}	Permeance$_i$/mol m^{-2} s^{-1} Pa^{-1}	$\alpha_{H_2/i}$
H_2	9.87×10^{-2}	1.95×10^{-6}	1
N_2	2.60×10^{-5}	5.14×10^{-10}	~3800
He	6.70×10^{-5}	1.32×10^{-9}	~1500

Furthermore, the permeated hydrogen purity did not vary significantly with WHSV being *ca.* 91%. Also in this case, no CO presence was noticed in the permeate side.

At the end of the whole experimental reaction campaigns, the permeation characteristics of the Pd/Al_2O_3 membrane have been checked again at T = 300 °C and ΔP = 1.0 bar. Table 9 reports the new ideal selectivities values, which are different from the fresh membrane; the permeability increased and the selectivity decreased by a factor of *ca.* 2. This probably occurred because of the effect of thermal cycles that greatly affect the gas permeation characteristics of the composite Pd-membrane.

4. Conclusions

The effect of the surface area and polarity ratio (related to the facet defects) of ZnO supports on the activity–selectivity of CuO/ZnO catalysts for MSR was studied. The ZnO surface area was varied by changing the calcination temperature of the prepared ZnO materials, whereas, its polarity ratio was modified using different Zn precursors, acetate or nitrate.

Both the copper surface area and the dispersion increase with the surface area of ZnO support. The polarity ratio of the ZnO carrier did not significantly affect copper dispersion but it influenced notably the reducibility of copper species. A higher polarity ratio of ZnO promotes the reducibility of copper oxide. This is attributed to a strong interaction between copper species and the *more polar* facets of ZnO, which are in higher proportion in the ZnO support with higher polarity ratio.

The activity of CuO/ZnO catalysts shows a marked dependence on the surface area of the ZnO supports, which in turn affects the dispersion of copper. In fact, those catalysts with higher surface area (and also Cu dispersion) also exhibit higher activity. Interestingly, the experimental results evidence that the selectivity of CuO/ZnO catalysts is closely related to the polarity ratio of the ZnO carriers: the selectivity increases with the polarity ratio, probably due to the presence of more selective Cu–ZnO sites at the Cu–ZnO polar interface. The $CuO/ZnO_{Ac\text{-}375}$ catalyst also shows a drastic improvement of selectivity as compared to commercial $CuO/ZnO/Al_2O_3$ sample. In fact, at similar methanol conversion the in-house catalyst has proven to be up to 90% more selective than the commercial sample.

Best performing catalyst $CuO/ZnO_{Ac\text{-}375}$ was further tested in a Pd-membrane reactor, made of a thin Pd-layer deposited on Al_2O_3 support. Two studies were performed, one concerning the catalyst performance in terms of methanol conversion and gas selectivity stability and the other concerning the MR performance in terms of hydrogen recovery and hydrogen permeate purity for various operating conditions.

During the first set experiments, the best result has been reached for 300 °C, 2.0 bar and WHSV = 2.73 h^{-1} with 97% of methanol conversion. Furthermore, a good stability of both conversion and gas selectivity was observed. The second set of experiments allowed to achieve a hydrogen recovery of *ca.* 75% and a hydrogen permeate purity higher than 90% at 330 °C, 2.5 bar and WHSV = 1.37 h^{-1}. This work pointed out that the Pd-based MR allows obtaining higher methanol conversions and a high purity permeate hydrogen, free of CO.

Acknowledgments

The authors would like to thank the European Union's Seventh Framework Programme (FP7/2007-2013) for the Fuel Cells and Hydrogen Joint Technology Initiative under grant agreement No [303476] due to the funding received for part of this work. This work was performed under the project "SYM – Produção de Metanol por Electrólise de Agua, usando Electrodos de Grafite" (ref. FCOMP-01-0202-FEDER-038899), financed by European Regional Development Fund (ERDF), through the Operational Program for Competitiveness Factors (POFC) in the National Strategic Reference Framework (NSRF), in the framework of the Incentive system for technology research and development. Dr. C. Mateos-Pedrero is grateful to the Portuguese Foundation for Science and Technology (FCT) for her Post-Doctoral Grant (Reference: SFRH/BPD/97114/2013). Prof. Y. Huang of Nanjing Tech-University (China) is particularly acknowledged for the preparation of Pd-composite membrane used in this work. The work of H. Silva was supported by FCT, grant SFRH/BD/45890/2008.

Appendix A. Supplementary data

Supplementary data associated with this article can be found, in the online version, at http://dx.doi.org/10.1016/j.apcatb.2015.02.039.

References

[1] S. Sá, H. Silva, L. Brandão, J.M. Sousa, A. Mendes, Catalysts for methanol steam reforming—a review, Appl. Catal. B: Environ. 99 (2010) 43–57.
[2] G.C. Chinchen, K.C. Waugh, The activity and state of the copper surface in methanol synthesis catalysts, Appl. Catal. 25 (1986) 101–107.
[3] S.T. Yong, C.W. Ooi, S.P. Chai, X.S. Wu, Review of methanol reforming-Cu-based catalysts, surface reaction mechanisms, and reaction schemes, Int. J. Hydrogen Energy 38 (2013) 9541–9552.
[4] M.S. Spencer, The role of zinc oxide in Cu/ZnO catalysts for methanol synthesis and the water–gas shift reaction, Top. Catal. 8 (1999) 259–266.
[5] M. Berens, F. Studt, I. Kasatkin, S. Kühl, M. Hävecker, F. Abild-Pedersen, S. Zander, F. Girgsdies, P. Kurr, B.L. Kniep, M. Tovar, R.W. Fischer, J.K. Nørskov, R. Schlögl, The active site of methanol synthesis over $Cu/ZnO/Al_2O_3$ industrial catalysts, Science 336 (2012) 893–897.
[6] Y. Kanai, T. Watanabe, T. Fujitani, T. Uchijima, J. Nakamura, The synergy between Cu and ZnO in methanol synthesis catalysts, Catal. Lett. 38 (1996) 157–163.
[7] A.M. Karim, T. Conant, A.K. Datye, Controlling ZnO morphology for improved methanol steam reforming reactivity, Phys. Chem. Chem. Phys. 10 (2008) 5584–5590.
[8] G.K. Smith, S. Lina, W. Laia, A. Datyeb, D. Xiec, H. Guo, Initial steps in methanol steam reforming on PdZn and ZnO surfaces: density functional theory studies, Surf. Sci. 605 (2011) 750–759.
[9] M.B. Boucher, S. Goergen, N. Yia, M. Flytzani-Stephanopoulos, Shape effects' in metal oxide supported nanoscale gold catalysts, Phys. Chem. Chem. Phys. 13 (2011) 2517–2527.
[10] M.B. Boucher, N. Yi, F. Gittleson, B. Zugic, H. Saltsburg, M. Flytzani-Stephanopoulos, Hydrogen production from methanol over gold supported on ZnO and CeO_2 nanoshapes, J. Phys. Chem.: C 115 (2010) 1261–1268.
[11] H. Silva, C. Mateos-Pedrero, C. Magén, D.A. Pacheco-Tanaka, A. Mendes, Simple hydrothermal synthesis method for tailoring the physicochemical properties of ZnO: morphology, surface area and polarity, RSC Adv. 4 (2014) 31166–31176.
[12] Y.M. Lin, M.H. Rei, Study on hydrogen production from methanol steam reforming in supported palladium membrane reactor, Catal. Today 67 (2001) 77–84.
[13] X. Hu, W. Chen, Y. Huang, Fabrication of Pd/ceramic membranes for hydrogen separation based on low-cost macroporous ceramics with pencil coating, Int. J. Hydrogen Energy 35 (2010) 7803–7808.
[14] Y. Huang, R. Dittmeyer, Preparation of thin palladium membranes on a porous support with rough surface, J. Membr. Sci. 302 (2007) 160–170.
[15] A.W. Li, J.R. Grace, C.J. Lim, Preparation of thin Pd-based composite membrane on planar metallic substrate part II. Preparation of membranes by electroless plating and characterization, J. Membr. Sci. 306 (2007) 159–165.
[16] S. Liguori, A. Iulianelli, F. Dalena, P. Pinacci, F. Drago, M. Broglia, Y. Huang, A. Basile, Performance and long-term stability of Pd/PSS and Pd/Al_2O_3 membranes for hydrogen separation, Membranes 4 (2014) 143–162.

[17] N. Itoh, Y. Kaneko, A. Igarashi, Efficient hydrogen production via methanol steam reforming by preventing back-permeation of hydrogen in a palladium membrane reactor, Ind. Eng. Chem. Res. 41 (2002) 4702–4706.
[18] S. Liguori, A. Iulianelli, F. Dalena, V. Piemonte, Y. Huang, A. Basile, Methanol steam reforming in an Al_2O_3 supported thin Pd-layer membrane reactor over $Cu/ZnO/Al_2O_3$ catalyst, Int. J. Hydrogen Energy 39 (2014) 18702–18710.
[19] A. Basile, Hydrogen production using Pd-based membrane reactors for fuel cells, Top. Catal. 51 (2008) 107–122.
[20] S. Sà, J.M. Sousa, A. Mendes, Methanol steam reforming in a dual-bed membrane reactor for producing PEMFC grade hydrogen, Catal. Today 156 (2010) 254–260.
[21] A. Iulianelli, T. Longo, A. Basile, Methanol steam reforming in a dense Pd–Ag membrane reactor: the pressure and WHSV effects on CO-free H_2 production, J. Membr. Sci. 323 (2008) 235–240.
[22] A. Iulianelli, T. Longo, A. Basile, Methanol steam reforming reaction in a Pd–Ag membrane reactor for CO-free hydrogen production, Int. J. Hydrogen Energy 33 (2008) 5583–5588.
[23] K. Ghasemzadeh, S. Liguori, P. Morrone, A. Iulianelli, V. Piemonte, A.A. Babaluo, A. Basile, H_2 production by low pressure methanol steam reforming in a dense Pd–Ag membrane reactor in co-current flow configuration: experimental and modeling analysis, Int. J. Hydrogen Energy 36 (2013) 16685–16697.
[24] S. Sà, H. Silva, Jose M. Sousa, A. Mendes, Hydrogen production by methanol reforming in a membrane reactor: palladium vs carbon molecular sieve membranes, J. Membr. Sci. 339 (2009) 160–170.
[25] A. Iulianelli, P. Ribeirinha, A. Mendes, A. Basile, Methanol steam reforming for hydrogen generation via conventional and membrane reactors: a review, Renew. Sust. Energy Rev. 29 (2014) 355–368.
[26] M.C.N. Amorim de Carvalho, F.B. Passos, M. Schmal, Quantification of metallic area of high dispersed copper on ZSM-5 catalyst by TPD of H_2, Catal. Commun. 3 (2002) 503–509.
[27] G.F. Froment, K.B. Bischoff, Chemical Reactor Analysis and Design, second ed., Wiley, New York, 1990.
[28] M. Muhler, L.P. Nielsen, E. Törnqvist, B.S. Clausen, H. Topsøe, Temperature-programmed desorption of H_2 as a tool to determine metal surface areas of Cu catalysts, Catal. Lett. 14 (1992) 241–249.
[29] S.G. Sanches, J. Huertas Flores, R.R. de Avillez, M.I. Pais da Silva, Influence of preparation methods and Zr and Y promoters on Cu/ZnO catalysts used for methanol steam reforming, Int. J. Hydrogen Energy 37 (2012) 6572–6579.
[30] L.-C. Wang, M. Y.-Mei Liu, Chen, Y. Cao, H.-Y. He, G.-S. Wu, W.-L. Dai, K.-N. Fan, Production of hydrogen by steam reforming of methanol over Cu/ZnO catalysts prepared via a practical soft reactive grinding route based on dry oxalate-precursor synthesis, J. Catal. 246 (2007) 193–204.
[31] B.L. Kniep, F. Girgsdies, T. Ressler, Effect of precipitate aging on the microstructural characteristics of Cu/ZnO catalysts for methanol steam reforming, J. Catal. 236 (2005) 34–44.
[32] H. Zhang, J. Sun, V.L. Dagle, B. Halevi, A.K. Datye, Y. Wang, Influence of ZnO facets on Pd/ZnO catalysts for methanol steam reforming, ACS Catal. 4 (2014) 2379–2386.
[33] M. Kurtz, N. Bauer, C. Buscher, H. Wilmer, O. Hinrinchen, R. Becker, S. Rabe, K. Merz, M. Driess, R.A. Fischer, M. Muhler, New synthetic routes to more active Cu/ZnO catalysts used for methanol synthesis, Catal. Lett. 92 (2004) 49–52.
[34] C. Baltes, S. Vukojevic, D. Schuth, Correlations between synthesis precursor, and catalyst structure and activity of a large set of $CuO/ZnO/Al_2O_3$ catalysts for methanol synthesis, J. Catal. 258 (2008) 334–344.
[35] S. Natesakhawat, J.W. Lekse, J.P. Baltrus, P.R. Ochodnicki, B.H. Howard, X. Deng, C. Matranga, Active sites and structure–activity relationships of copper-based catalysts for carbon dioxide hydrogenation to methanol, ACS Catal. 2 (2012) 1667–1676.
[36] C. Pacholski, A. Kornowski, H. Weller, Self-assembly of ZnO: from nanodots to nanorods, Angew. Chem. Int. Ed. 41 (2002) 1188–1191.
[37] O. Dulub, M. Batzill, U. Diebold, Growth of copper on single crystalline ZnO: surface study of a model catalyst, Top. Catal. 36 (2005) 65–76.
[38] C. Wöll, The chemistry and physics of zinc oxide surfaces, Prog. Surf. Sci. 82 (2007) 55–120.
[39] C.T. Campbell, C.H.F. Peden, Oxygen vacancies and catalysis on ceria surfaces, Science 309 (2005) 713–714.
[40] M.P. Hyman, V.M. Lebarbie, Y.W. Abhaya, K. Datye, J.M. Vohs, A comparison of the reactivity of Pd supported on ZnO($10\bar{1}0$) and ZnO(0001), J. Phys. Chem. C 113 (2009) 7251–7259.
[41] B. Halevi, E.J. Peterson, A. DeLaRiva, E. Jeroro, V.M. Lebarbier, Y. Wang, J.M. Vohs, B. Kiefer, E. Kunkes, M. Havecker, M. Behrens, R. Schlögl, A.K. Datye, Aerosol-derived bimetallic alloy powders: bridging the gap, J. Phys. Chem. C 114 (2010) 17181–17190.
[42] B. Halevi, E.J. Peterson, A. Roi, A. DeLaRiva, E. Jeroro, F. Gao, Y. Wang, J.M. Vohs, B. Kiefer, E. Kunkes, M. Havecker, M. Behrens, R. Schlögl, A.K. Datye, Catalytic reactivity of face centered cubic PdZnα for the steam reforming of methanol, J. Catal. 291 (2012) 44–54.